Superhydrophobicity of nanofibrillated cellulose materials through polysiloxane nanofilaments

Author(s):
Orsolini, Paola; Antonini, Carlo; Stojanovic, Ana; Malfait, Wim J.; Caseri, Walter; Zimmermann, Tanja

Publication date:
2018-02

Permanent link:
https://doi.org/10.3929/ethz-b-000272852

Originally published in:
Cellulose 25(2), https://doi.org/10.1007/s10570-017-1636-8

Cellulose (2018) 25:1127–1146
https://doi.org/10.1007/s10570-017-1636-8

ORIGINAL PAPER

Superhydrophobicity of nanofibrillated cellulose materials through polysiloxane nanofilaments

Paola Orsolini · Carlo Antonini · Ana Stojanovic · Wim J. Malfait · Walter R. Caseri · Tanja Zimmermann

Received: 14 August 2017 / Accepted: 18 December 2017 / Published online: 26 December 2017

Abstract The wetting behavior of nanofibrillated cellulose (NFC) was drastically changed from hydrophilic to superhydrophobic, achieving limited contact angle hysteresis. Remarkably, superhydrophobicity was attained for a variety of morphologies, namely dense and porous films, foams and powders, thus exploiting a wide spectrum of cellulose manifestations. The superhydrophobic behavior resulted from the combined action of hydrophobic polysiloxane nanofilaments, formed by controlled reaction of methyltrichlorosilane with water at the surface of NFC fibrils, and the NFC substrates surface morphology, established by various drying methods of the nanofibrils. In particular, the optimal conditions for polysiloxane nanofilaments growth, with identification of various regimes of coating versus nanofilaments growth, were identified. Depending on the morphology, we demonstrated that modified NFC materials can act multiple roles, such as superhydrophobic liquid-infused lubricating surfaces, filters for dodecane drops capture from a nebulized dodecane/water mixture, hydrocarbon absorption from an aqueous phase, with absorbance capacity as high as 50 $g_{dodecane}/g_{foam}$, and beds to separate hydrocarbon/water mixture. As such, the versatile combination of two materials with nanoscale features (nanocellulose and nanofilaments), which provide multi-tier topography and unprecedented wetting characteristics, can serve for all those applications, in which liquid mixture behavior (e.g. water/hydrocarbon) needs to be controlled.

Keywords Microfibrillated cellulose · Superhydrophibicity · Methyltrichlorosilane · MTCS · SLIPS · LIS · Oil absorber · Foams

Electronic supplementary material The online version of this article (https://doi.org/10.1007/s10570-017-1636-8) contains supplementary material, which is available to authorized users.

P. Orsolini (✉) · C. Antonini · T. Zimmermann (✉)
Applied Wood Materials, Swiss Federal Laboratories for Materials Science and Technology (Empa), Dübendorf, Switzerland
e-mail: paola.rsln@gmail.com

T. Zimmermann
e-mail: tanja.zimmermann@empa.ch

P. Orsolini · W. R. Caseri
Multifunctional Materials Laboratory, ETH-Zürich, Zurich, Switzerland

A. Stojanovic · W. J. Malfait
Building, Energy, Materials and Components, Swiss Federal Laboratories for Materials Science and Technology (Empa), Dübendorf, Switzerland

Introduction

Nanofibrillated cellulose (NFC) is a biodegradable, renewable, cellulose-derived material composed of high aspect-ratio nanofibers. Notably, the production of NFC has been scaled up and the material is

nowadays available as a commodity. NFC can be processed to films with barrier properties against vapors or gases (Syverud and Stenius 2009; Spence et al. 2011; Lavoine et al. 2012), as films for oil/water separation (Zhou et al. 2013), and as foams for oil absorption in water (Jin et al. 2011a; Korhonen et al. 2011; Cervin et al. 2012; Payne et al. 2012; Zhang et al. 2014; Sai et al. 2015), or for thermal insulation (Zhao et al. 2015). In all those applications, it is essential to control the wetting properties of cellulose. NFC is inherently hydrophilic because of the hydroxyl groups on its surface (Samyn 2013), provided by both cellulose and hemicelluloses. Wetting modification can be achieved by chemical reaction with hydroxyl groups of NFC, which are available in larger quantities than in pristine cellulose fibers. Several approaches were used to impart hydrophobicity to cellulose and NFC, varying from grafting techniques to layer-by-layer and solution treatments (Samyn 2013). Zhang et al. (2014) recently reported a water-based silylation process to fabricate hydrophobic, flexible, and ultra-lightweight nanocellulose sponges, by freeze-drying water suspensions of NFC modified with a homogeneous silane monolayer. The sponges were hydrophobic, with contact angles in the range of 110°–140°, but not superhydrophobic. Similar results were achieved by Korhonen et al. (2011), who fabricated hydrophobic cellulose foams through atomic layer deposition of a uniform 7 nm-thick titanium dioxide layer, and by Sai et al. (2015) through silylation of bacterial cellulose. In specific conditions for other classes of materials, it was shown that it is possible to achieve superhydrophobicity, a property traditionally attributed to surfaces with high advancing contact angles ($\theta_A > 150°$) and low contact angle hysteresis ($\Delta\theta < 10°$); the contact angle hysteresis denotes the difference between the advancing, θ_A, and receding contact angles, θ_R, which are measured by quasi-statically expanding or contracting, respectively, a drop on a horizontal surface. Here we designate $\theta_R > 135°$ as a threshold for superhydrophobicity, on the basis of previous experimental (Rioboo et al. 2012; Antonini et al. 2013; Schellenberger et al. 2016) and theoretical (Li and Amirfazli 2005) results. Indeed, Rioboo et al. (2002) investigated the controlled sliding motion of water drops on horizontal surfaces, showing that high mobility of drops depends essentially on the receding contact angle, θ_R, and is achieved when $\theta_R > 135°$, and Schellenberger et al. (2016) suggested the use of the receding contact angle for appropriate characterization of super-liquid-repellent surfaces.

NFC substrates with a monolayer coating without additional topographical features, as in Ref. Zhang et al. (2014), can be hydrophobic, but not necessarily superhydrophobic. Notably, superhydrophobicity is achieved by a combination of surface chemistry and topography (Kim 2008; Flemming et al. 2009). The existence of micro- and nano-asperities allows trapping of air pockets at the substrate/liquid interface, minimizing the contact area between the two. Hitherto, most of the approaches have relied only on the use of hydrophobic functional groups, including alkyl-, alkoxy- and perfluorinated silanes, which comprise end groups with gradually reduced surface free energies, such as $–CH_2–$, $–CH_3$, $–CF_2–$, $–CF_2H$ and $–CF_3$ groups (Nishino et al. 1999; Zhang et al. 2008). As the specific surface free energy of fluorinated groups is lower than that of hydrocarbon groups, it is often anticipated that fluorinated groups are required to achieve superhydrophobicity. The preparation of superhydrophobic surfaces on silicon substrates by the formation of a fluorine-free polysiloxane network was first reported by Gao and McCarthy (2006). The authors added topographical features by the vertical polymerization of methyltrichlorosilane (MTCS, with 1D polysiloxane nanostructure imparting superhydrophobicity as discussed in Artus and Seeger (2014). Subsequently, Seeger and co-workers (Artus et al. 2006; Zimmermann et al. 2008) demonstrated the potential of such approach for a wide range of substrates, including metals and ceramics (Artus et al. 2006), polyester (Zhang and Seeger 2011), and cotton fibers with diameters in the order of 10 μm (Zimmermann et al. 2008); however, high contact angle hysteresis for wood ($\Delta\theta > 70°$) was reported. Maitra et al. (2014) took advantage of multiple hydrophobic layers, including self-assembled monolayers, thin films, and polyalkylsilsesquioxanes to functionalize aluminum substrates, and to achieve robust superhydrophobicity under adverse conditions. The multilayered surface exhibited simultaneous chemical stability, mechanical durability and drop impalement resistance, which is important to prevent the undesirable wetting transition from the Cassie-Baxter to the Wenzel regime (Bormashenko 2013).

Patankar (2009) theoretically anticipated that rough surfaces made of hydrophilic material can own by themselves a hydrophobic component.

Based on the former considerations, the goal of this study is to achieve extreme superhydrophobicity of NFC, an intrinsically hydrophilic material, by combining different substrate roughness and porosity, together with the MTCS-based functionalization approach to form a three-dimensional polyalkylsilsesquioxane (polysiloxane, for simplicity) network by polymerization of methyltrichlorosilane (MTCS) into nanofilaments. Although the chemical modification with methyltrichlorosilane has been already applied on cellulosic materials through vapor-phase deposition processes (Cunha et al. 2010; Tejado et al. 2014; Zheng et al. 2014; Jiao et al. 2016), leading to superhydrophobicity, formation of MTCS nanofilaments via a solution method for superhydrophobic nanocellulose has not been described so far. A similar concept was proposed by Guo et al. (2016) based on the chemical modification of NFC films with vinyltrichlorosilane (VTCS), however a clear formation of polysiloxane filaments was not shown.

In our work, for the first time a superhydrophobic wetting state was reached by combining nanocellulose topography together with low specific surface free energy and micro and nanoscale asperities introduced by nanofilaments, through a single step fabrication process. The novel combination of known materials, such as NFC and chlorosilanes, led to superhydrophobic materials with extremely low hysteresis of the contact angles, rarely reported so far. The experiments include optimization of the formation of polysiloxane nanofilaments on dense and porous NFC films and NFC foams. We also demonstrate the potential use of NFC substrates as superhydrophobic liquid-infused lubricating surfaces, known as SLIPS or LIS in the literature (Lafuma and Quere 2003; Wong et al. 2011; Rykaczewski et al. 2013), as well as filters and oil absorbers. In addition, we prove functionalization of suspended NFC fibers by methyltrichlorosilane, to obtain superhydrophobic NFC-based powders.

Experimental section

Materials and methods

Methyltrichlorosilane (MTCS) and anhydrous toluene were purchased from Sigma (Switzerland), and toluene Analar Normapure from VWR (Switzerland).

NFC was produced from a water-based suspension at 2 wt% of elemental chlorine free (ECF) cellulose pulp (Zellstoff Stendal, Germany), containing spruce (60–70%) and pine fibers (30–40%), as reported elsewhere (Orsolini et al. 2015). The sugar analysis revealed for ECF pulp a glucose content of 81.3%, a hemicellulose content of 4.7% (mannose), 0.7% (arabinose), 0.3% (galactose), 6.7% (xylose), respectively, and a soluble lignin concentration of 0.3% with a total ash content of 0.3%. The sum of those compounds does not reach 100% due to insoluble lignin fractions and other wood extractives. The NFC was not chemically treated (i.e. oxidized) before mechanical disintegration.

Preparation of dense and porous substrates

Dense NFC films with diameter of 5 cm and grammage of 30 g/m^2 were produced from a 2 wt% NFC suspension in deionized water, through a vacuum filtration process on a metal mesh (mesh 325 × 2300, warp × weft 0.035 mm × 0.025 mm), and subsequently dried in a hot press for 20 min at 120 °C. Porous NFC films with diameter of 5 cm and grammage of 30 g/m^2 were produced by vacuum filtration and subsequently by supercritical drying from a 2 wt% NFC suspension in ethanol; the process was performed in a supercritical point dryer E3000 (Quorum Technologies, USA) and consisted of solvent exchange from ethanol to liquid CO_2 overnight, followed by drying at supercritical conditions (35 °C and 1000 bar).

NFC foams were prepared by freeze-drying from NFC suspension in deionized water: 250 ml of 1 wt% NFC suspension were poured into a squared copper holder (15 × 15 cm) and frozen by submerging in liquid nitrogen for 30 min. The holders were inserted afterwards in a freeze-dryer and vacuum was maintained for at least 72 h and until no variation in relative pressure was observed in the chamber (pressure in the order of 1 Pa) when excluding the pumping system, indicating a dry sample.

Functionalization of NFC substrates

Samples of NFC substrates (dense and porous films as well as foams) were pre-conditioned for at least 10 days at different relative humidity in desiccators, in presence of oversaturated aq. salt solutions (Rockland

1960) as follows: 11%RH (LiCl solution), 43%RH (K_2CO_3 solution), 65%RH ($NaNO_2$ solution) and 85%RH (KCl solution). After pre-conditioning, the substrates were removed from the desiccators and dipped into a toluene Analar Normapure based methyltrichlorosilane solution, at different concentrations ranging from 0.0015 to 2.7 M. The functionalization reactions were performed at static conditions, for $\sim$ 17 h, in a sealed chamber. After reaction, samples were rinsed by dipping into toluene and ethanol, at various soaking times (for details see SI, Section 1). As a last step, samples were dried in an oven at 100 °C for 10 min (films), or for 15 min (foams).

In addition, suspended NFC fibers were also functionalized. First, the NFC suspension was solvent-exchanged from water to toluene via ethanol. The process consisted of subsequent cycles, composed of: (1) centrifugation of 850 mL of a 2 wt% suspension at 5000 rpm for 15 min, (2) removal of the supernatant liquid after decantation, (3) re-dispersion of the NFC in 700 mL ethanol (2 cycles) and 700 mL toluene (2 cycles), (4) NFC redispersion using an Ultraturrax T25 disperser (IKA, Germany) in 700 mL anhydrous toluene (Sigma, Switzerland). The final dispersion contained 4.3% NFC dry matter. To carry out the reaction, 0.1 g NFC dry matter was placed in a three-necks round flask and 50 mL of fresh anhydrous toluene were added. The flask was closed with septa and flushed with nitrogen until the residual water content in the toluene solution was below 100 ppm, as determined in aliquots of the solution by means of a Karl-Fischer titrator. Subsequently, 50 mL NFC suspensions were functionalized by adding different quantities of methyltrichlorosilane directly to the toluene to obtain concentrations of 0.006, 0.025 and 1 M methyltrichlorosilane. The reactions were carried out at room temperature, by stirring at 550 rpm for 17 h. The final washing was performed by centrifugation at 5000 rpm for 10 min of 45 mL volumes, decantation, removal of the supernatant and re-dispersion in fresh solvent. The cycles were repeated as follows: first, we removed the reagent medium and unreacted silane, second we replaced with 35 mL volume of fresh toluene and redispersed the reaction product for 2 times, then we performed solvent exchange with 35 mL of a 50:50 mixture toluene:ethanol and eventually with 45 mL ethanol for 2 times.

Nitrogen adsorption

Nitrogen adsorption at 77 K was measured with a Micromeritics 3 Flex (Micromeritics, Germany). To determine the specific surface area the method of Brunauer–Emmett–Teller (BET) was employed, respectively. NFC substrates were outgassed at 90 °C in ultimate vacuum of 3.75×10^{-10} mmHg for 16 h prior the measurements.

Scanning electron microscopy

Scanning electron microscopy (SEM) was performed on all substrates (films, foams and modified NFC) using a Fei Nova Nanosem 230 Instrument (Fei, USA). On foams and porous films, SEM imaging was combined with energy dispersive X-ray (EDX) spectroscopy.

Infrared spectroscopy

Fourier-transform infrared spectroscopy (Tensor 27, Bruker, Germany) as well as ATR-FTIR microscopy (Hyperion 2000, Bruker, Germany) were performed on dense films. To ensure reproducibility, dense films were functionalized in triplicates, with each film analyzed at 5 spots and their spectra averaged. Normalization with respect to the asymmetric stretching of the C–O–C at β-glucosidic linkage (Oh et al. 2005) at 897 cm^{-1} was performed to evaluate the extent of the chemical modification.

Solid-state NMR spectroscopy

Magic Angle Spinning (MAS) NMR spectra were collected following established procedures (Malfait et al. 2015) and the spectra were processed with matNMR (van Beek 2007). The data were acquired with a Bruker Avance III spectrometer equipped with a wide-bore 9.4 T magnet, corresponding to ^{1}H, ^{13}C and ^{29}Si Larmor frequencies of 400.2, 100.6 and 79.5 MHz, respectively. Single pulse ^{1}H spectra were collected with 2.5 mm zirconia rotors, a MAS rate of 24 kHz and a recycle delay of 10 s (for a *T1* relaxation time < 1 s). The background spectrum of an empty rotor was subtracted from the signal. ^{1}H-^{13}C and ^{1}H-^{29}Si cross polarization (CP) spectra were collected with 7 mm zirconia rotors at a MAS rate of 4 kHz and

a recycle delay of 2 s. The contact times were set to 2 and 5 ms for the ^{13}C and ^{29}Si CP spectra, respectively.

Thermogravimetric analysis

Thermogravimetric analysis (TGA) was performed with a Netzsch TG 209F1 (Netzsch, Germany), using two different procedures: (1) at increasing temperature, with a temperature rate of 20 °C/min under nitrogen, up to 900 °C, and (2) with the same temperature rate, under nitrogen up to 600 °C, and subsequently under air.

Contact angle measurements

Advancing and receding contact angles (θ_A and θ_R, respectively) were measured using the sessile drop method on dense and porous films, by expansion and contraction of the volume of a sessile drop (volume up to 10 µL) on a horizontal sample. Measurements were performed with a contact angle measurement system (OCA 30 and 35, Dataphysics), and the image post-processing of contact angle evolution was performed using the Datasystem SCA20 image analysis software. Contact angle measurements were performed after ultrasonication for 30 s at room temperature.

Dodecane and water behavior at the cellulose interface (SLIPS, absorption, filtration)

First, dodecane (VWR, Switzerland) was stained in red by adding 0.01 g of Sudan III (standard Fluka, Fluka AG) to 1 L of dodecane and 0.01 g/L of Neolan Blau (CIBA GEIGY) to 1L of milli-Q water. Staining was required to enhance the contrast between the two liquid phases. Dense films were exposed to dodecane to produce a self-infused lubricating film and the self-cleaning ability toward water was investigated by means of a water drop experiment. The latter was performed on horizontal surfaces. Porous films were exposed to a nebulized mixture of dodecane and water and the separation ability visually assessed.

Foams were used as sorbent for hydrocarbon and immersed in water. The foam mass was measured before (m_{dry}) and after dodecane absorption (m_{uptake}) and the dodecane absorption capacity C was subsequently evaluated with Eq. 1:

$$C = \left(m_{uptake} - m_{dry}\right)/m_{dry} \quad (1)$$

The recyclability of the foams upon repeated absorption cycles was assessed, as reported elsewhere (Zhang et al. 2014), utilizing toluene as solvent.

Modified NFC powder was placed in a capillary glass pipette on a metal mesh support and subjected to a flow of a dodecane/water biphasic mixture to visually evaluate their oleophilicity after chemical modification.

Results and discussion

To prepare superhydrophobic NFC, the material was exposed to methyltrichlorosilane (MTCS), as schematically illustrated in Fig. 1a.

In the following, we initially present the optimization process to achieve best superhydrophobic properties by controlling several parameters, such as: (1) the drying method for substrate preparation, (2) methyltrichlorosilane concentration in the solution during the functionalization step, and (3) the effect of relative humidity of the cellulosic substrate, controlled by NFC storage in desiccators containing different over saturated salt solutions. NFC substrate surfaces with different specific surface areas (SSA) measured by nitrogen adsorption were employed: dense films (SSA < 2 m^2/g) and porous films (SSA of $\sim$ 170 m^2/g), foams (SSA of $\sim$ 20 m^2/g), and cellulose nanofibers (SSA not possible to measure due to hornification, to be noticed that in solvent NFC maximizes their SSA). The unmodified substrates are shown in Fig. 1b–e, respectively. Applications for each class of material are also presented.

Dense films

Unmodified NFC dense films with grammage of 30 g/m^2 were employed as model samples to evaluate the growth of methyltrichlorosilane-derived filaments on nanocellulose at different silane concentrations. For this purpose, dense films were selected because their dense structure and porosity below 5% (Orsolini et al. 2015) provides compact surfaces, with a high surface density of reactive groups (alcohol groups of cellulose). Notably, chemical reaction proceeds mainly at the substrate surface, where the methyltrichlorosilane interacts with OH groups: water adsorbed on the NFC surface is readily available for the hydrolysis of Si–Cl

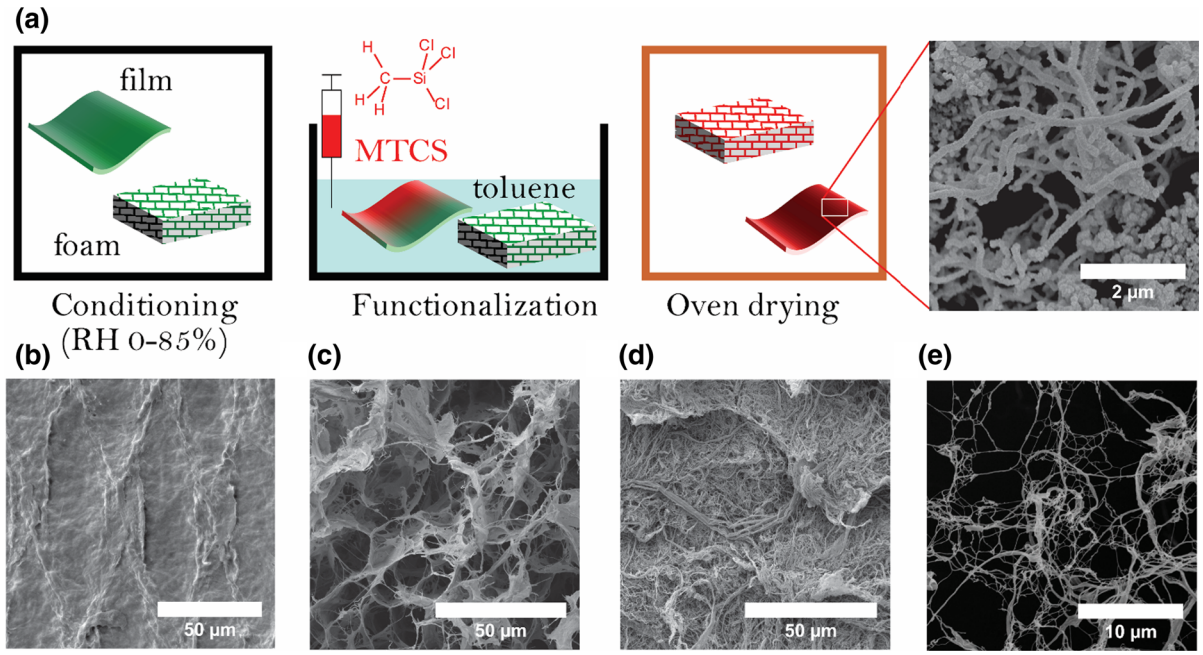

Fig. 1 **a** Schematic illustration of the chemical modification of NFC with polysiloxane nanofilaments, SEM images of **b** a dense film, **c** a foam, **d** a porous film and **e** suspended NFC

bonds in MTCS and subsequent condensation of the formed Si–OH groups. As such, the influence of adsorbed water in the NFC was investigated: substrates were conditioned at different relative humidity (%RH) and chemically modified with a constant concentration of 0.4 M methyltrichlorosilane.

Scanning electron microscopy (SEM)

We observed that relative humidity between 43%RH and 65%RH was optimal to obtain a homogeneous surface modification (Supplementary material, Figure S1); in case of cellulose conditioning at low humidity (viz. 11%RH), minor coverage of the surface was achieved. At the opposite extreme of conditioning at high humidity (85%RH), heterogeneous structures such as microbeads formed. This is in agreement with the findings of Khoo et al. (2008), Jin et al. (2011b) and Stojanovic et al. (2013) on other hydroxylated surfaces. Although for both substrates preconditioning at 43%RH and 65%RH polymer nanofilaments were formed, we chose to operate at a value of 43%RH for the subsequent investigations, as this humidity is close to environmental humidity in our laboratories.

Figure 2a shows curly entangled polysiloxane nanofilaments on a dense NFC film formed after treatment with 0.025 M solution of methyltrichlorosilane at 43%RH. Filaments have a length of a few micrometers, and diameters in the nanometer range. As reported in a previous work of Cunha et al., filaments can originate from three main mechanisms: horizontal polymerization, covalent attachment on OH groups and vertical polymerization of MTCS (Cunha et al. 2010). The polysiloxane thickness is difficult to determine. Attempts have been made by Stojanovic et al. on a smooth substrate, showing that the layer thickness can vary between 60 nm–5 µm depending on the reaction conditions (Stojanovic 2014). When a water drop is placed on the modified film, a remarkable water-repellent behavior can be visualized, with advancing and receding contact angles of $\sim$ 150° to 160° and low drop capillary adhesion, a manifestation of low contact angle hysteresis (Fig. 2b).

Fourier-transform infrared spectroscopy (FTIR)

We further screened the effect of methyltrichlorosilane concentration on the formation of polysiloxane nanofilaments at 43%RH. The effectiveness of the reaction was evaluated by ATR-FTIR spectroscopy (Fig. 3a). Compared to unmodified NFC, the modified samples showed peaks at 781 and 1270 cm^{-1},

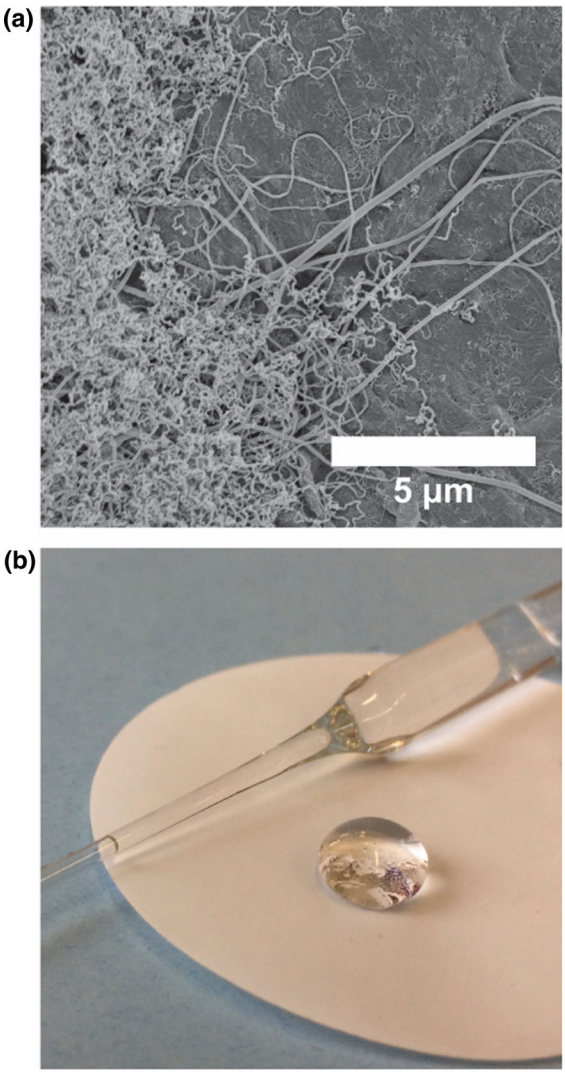

Fig. 2 **a** SEM micrograph depicting the formation of polysiloxane nanofilaments on a dense NFC film; **b** a water drop deposited at a surface modified with 0.025 M methyltrichlorosilane

attributed respectively to Si–O–Si and Si–CH_3 bending vibrations (Cunha et al. 2010). To allow comparison of different samples, peak intensities at 781 cm^{-1} (see Fig. 3a_3) and 1270 cm^{-1} (see Fig. 3a_2) were normalized to the peak intensity at 897 cm^{-1} (asymmetric stretching of the C–O–C). Results showed monotonic increase in the 781 and 1270 cm^{-1} peak intensities for exposure to silane concentration up to 0.1 M, above which signal saturation was observed. This trend can be interpreted by assuming saturation of the reactive groups on the substrate for reactions at concentrations of 0.1 M and above.

Dynamic water contact angle and scanning electron microscopy (SEM)

For methyltrichlorosilane concentrations of 0.0015 and 0.006 M, receding contact angle values were well below those of the advancing contact angles, and also showed large deviations. Both attributes are characteristic of highly heterogeneous substrates, causing contact line pinning upon drop retraction. Heterogeneity was also evident in SEM images, where agglomerated polysiloxane structures were evident (Fig. 3c, left). However, surfaces treated with higher concentrations of methyltrichlorosilane (above 0.1 M, Fig. 3b) showed only little differences between θ_A and θ_R (less than 5°) and small standard deviation, indicating a very homogeneous surface. Indeed, SEM images of such surfaces at 0.4 M methyltrichlorosilane showed a homogeneous distribution of polysiloxane structures (Fig. 3c, right).

Besides achieving similar contact angles by changing the silane concentrations, different intensities of the ATR-FTIR (semi-quantitative analysis) characteristic peaks with methyltrichlorosilane concentrations were observed; this can be explained by different polymerization pathways of the silane to form its 3-D structure.

ATR-FTIR microscopy and SLIPS evaluation

To further confirm the observed increase of surface homogeneity for increasing silane concentration, ATR-FTIR microscopy mapping was employed, to detect the distribution of the Si–O–Si peak intensity at 781 cm^{-1} on the sample surface (Fig. 4a, b) to reveal on which surface sports the coupling of methyltrichlorosilane on cellulose occurred. A 3-D mapping of the intensity is generated when scanning surface areas of 420 × 520 µm (21.84 mm^2), investigated in 144 positions in total. While the sample modified with 0.006 M methyltrichlorosilane (i.e. lowest concentration) resulted in uneven intensity of the peak at 781 cm^{-1} (Fig. 4a) corresponding to a non-homogeneous coupling, the sample modified with 0.4 M MTCS (i.e. highest concentration) exhibited a uniform signal all over the surface, indicating chemical homogeneity at a macroscopic level (Fig. 4b). Dense films

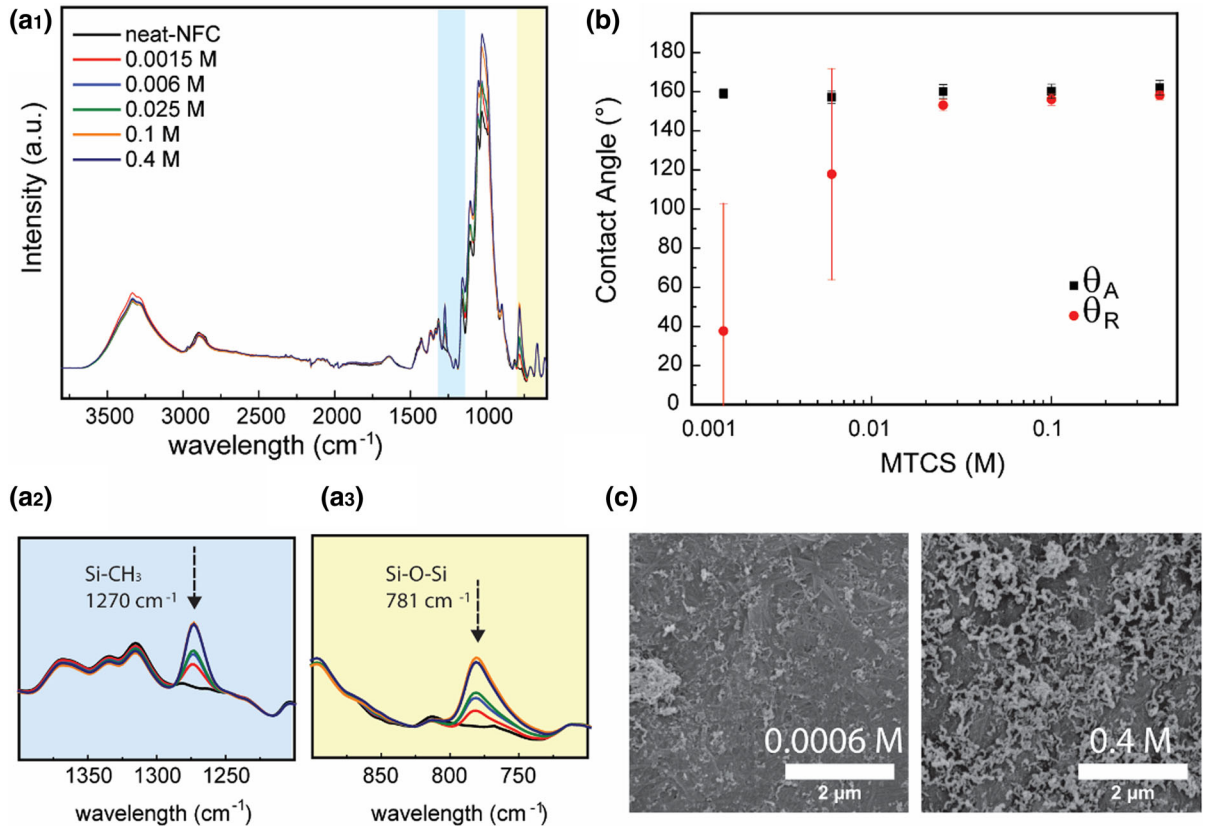

Fig. 3 Characterization of dense films modified with methyltrichlorosilane film: $\mathbf{a_1}$ ATR-FTIR spectra before and after modification with various concentrations of silane; $\mathbf{a_{2-3}}$ magnification of ATR-FTIR spectra around wavelengths of 1270 and 781 cm^{-1}, same legend as $\mathbf{a_1}$; **b** advancing (θ_A) and receding (θ_R) contact angle values for films modified with methyltrichlorosilane at various concentrations; **c** SEM images of a film modified with 0.0015 M (left) and 0.4 M (right) methyltrichlorosilane

were also infused with dodecane to assess the potential use of films as superhydrophobic liquid-infused lubricating surfaces (SLIPS/LIS).

Water contact angles as high as 105° ± 2°, with practically negligible hysteresis, were measured. An example is shown in Fig. 4c, confirming the water repellent behavior of dodecane infused NFC surfaces. The phenomenon can be macroscopically visualized in Fig. 4d, where the higher affinity of MTCS-modified NFC dense films to apolar liquids (transparent dodecane) compared to water (blue-stained drops) is evident. Displacement of infused liquids from the porous substrate may occur and limit the durability of liquid-infused surfaces. As an example, displacement may occur by other liquids or by Marangoni convection in case of thermal gradients. Assessing and optimizing the durability of the liquid-infused cellulose-based dense films is beyond the scope of the current paper. Nonetheless, we refer the reader to other studies (Anand et al. 2012; Smith et al. 2013), where optimization of durability has been discussed, depending on liquid properties and surface operating conditions.

In the following section, we present the extension of MTCS to porous films, foams and toluene-suspended NFC-fibers.

Porous films

Scanning electron micoscopy

Unmodified porous films with grammage of 30 g/m^2 were obtained from NFC supercritical drying, and their structure is shown in Figs. 1d and 5a. Compared to dense films of the same grammage, porous films containing the same NFC mass had a specific pore

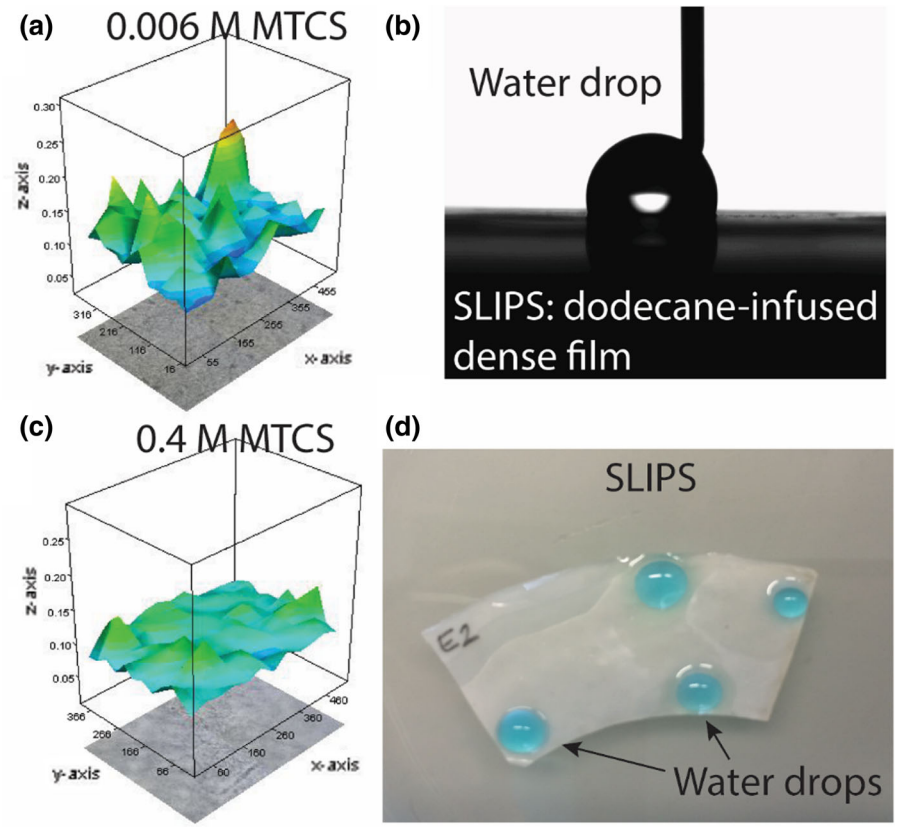

Fig. 4 Three-dimensional mapping of the peak intensity of the Si–O–Si vibration at 781 cm^{-1} for NFC films, as measured by FTIR: **a** samples treated with 0.006 M and **b** with 0.4 M methyltrichlorosilane; **c** Contact angle measurement of a water drop deposited on a dodecane-infused dense film and **d** an image of a superhydrophobic liquid-infused lubricating surface (SLIP/LIS) repelling water drops (stained in blue, unstained oil is transparent). (Color figure online)

volume of 0.7 cm^3/g and specific surface area of 175 m^2/g. Porous films were subject to modification by methyltrichlorosilane at different concentrations in toluene, with fixed pre-conditioning at 43%RH. SEM images in Fig. 5b–f show the porous films surfaces after functionalization, covered with polysiloxane nanofilaments. The nanofilaments homogeneity and coverage strongly depended on the applied methyltrichlorosilane concentration. At low concentration (0.025 M, Fig. 5b) only a few regions underwent modification, whereas at higher concentrations (0.1, 0.4 and 1.2 M, Fig. 5c–e), abundant polysiloxane nanofilaments coated the film surface. At 2.7 M methyltrichlorosilane concentration (Fig. 5f), the formation of rough heterogeneous structures instead of nanofilaments was observed.

Dynamic water contact angles

Contact angle measurements confirmed the visual information from SEM: advancing contact angles were high (in the range 157°–163°) for all samples exposed to methyltrichlorosilane concentrations between 0.025 and 2.7 M (Fig. 6). However, only in the concentration range between 0.1 and 0.4 M, the receding contact angles were also high ($\sim$ 150°) and close to the advancing contact angles, with small standard deviation and a low contact angle hysteresis ($\Delta\theta < 10°$): this indicates superhydrophobicity and high surface homogeneity has been reached.

Scanning electron microscopy (SEM) and X-ray dispersive spectroscopy (EDX)

SEM imaging coupled with EDX line-scans was performed to trace the presence of silicon across the film thickness and demonstrate the presence of polysiloxane. Six positions were analyzed from the top-surface to the bottom-surface (blue arrow pointing downward in Fig. 7a) and the EDX spectra in each position recorded (Fig. 7b).

The superhydrophobic properties of modified porous films can be used to separate biphasic mixtures of hydrophobic and hydrophilic liquids, based on

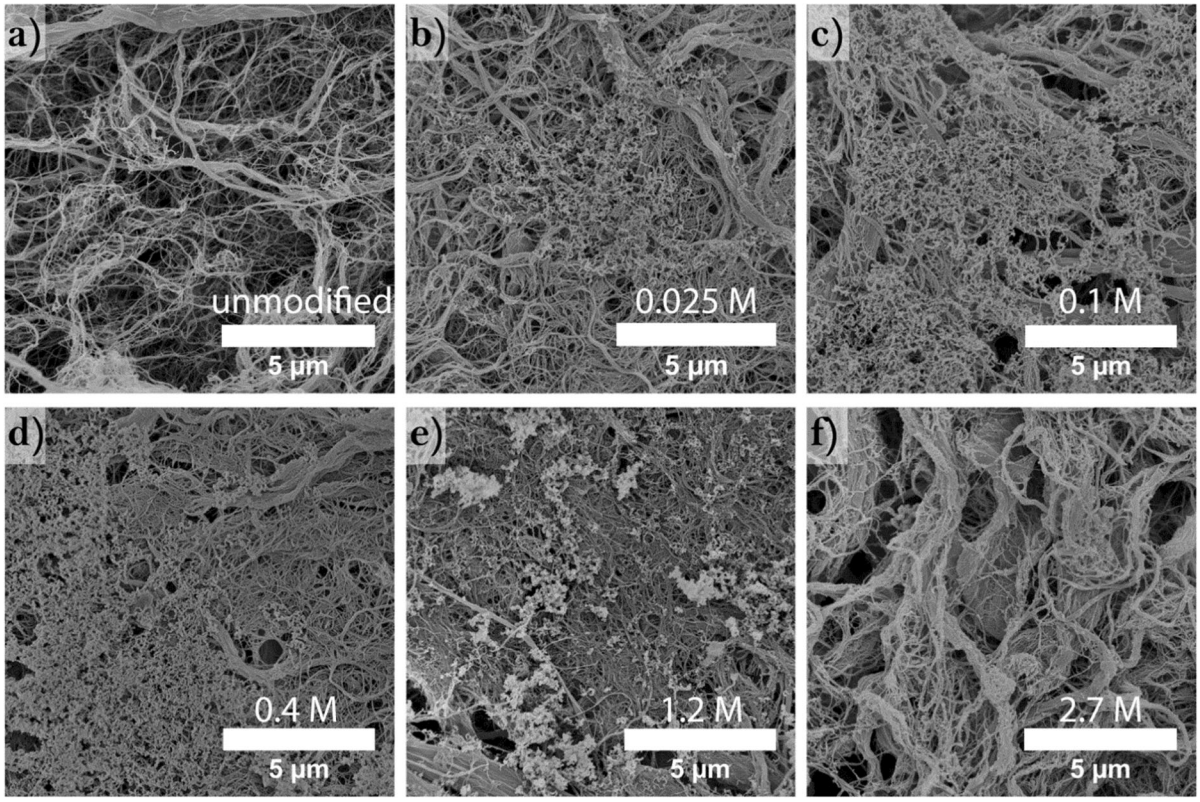

Fig. 5 SEM images of **a** unmodified porous films and porous films exposed to methyltrichlorosilane at a concentration of **b** 0.025 M, **c** 0.1 M, **d** 0.4 M and **f** 2.7 M

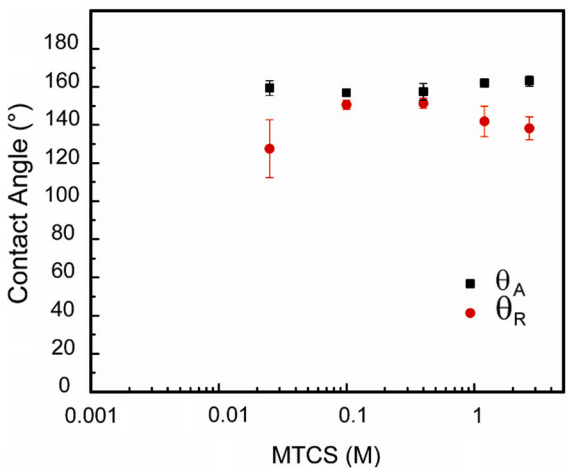

Fig. 6 Advancing (θ_A) and receding (θ_R) contact angle values for the same substrate (value of unmodified films could not be measured due to fast water drop soaking)

preferential wetting of one liquid. When superhydrophobic porous films were exposed to a nebulized mixture of 50:50 vol:vol dodecane (red-stained) and water (blue-stained), water drops formed, coalesced and slid down the film surface, whereas dodecane penetrated into the film and was retained (Fig. 7c). A movie of the experiment is available as supplementary material (SI, MOV1). An application of such material can be envisaged in downstream filtration units of water vapors exhaust outlets, containing entrained organic liquids drops to be removed.

Foams

X-ray dispersive spectroscopy (EDX)

Nanocellulose foams (thickness of about 1 cm) prepared by freeze-drying had a specific surface area of 16 m^2/g and specific pore volume (measured to a maximum pore size of 300 nm) was 0.1 cm^3/g. The SEM image in Fig. 1c discloses that the unmodified foams offered a combination of nano- and microporosity, corresponding to the known reported ice-templated structure obtained as a consequence of the

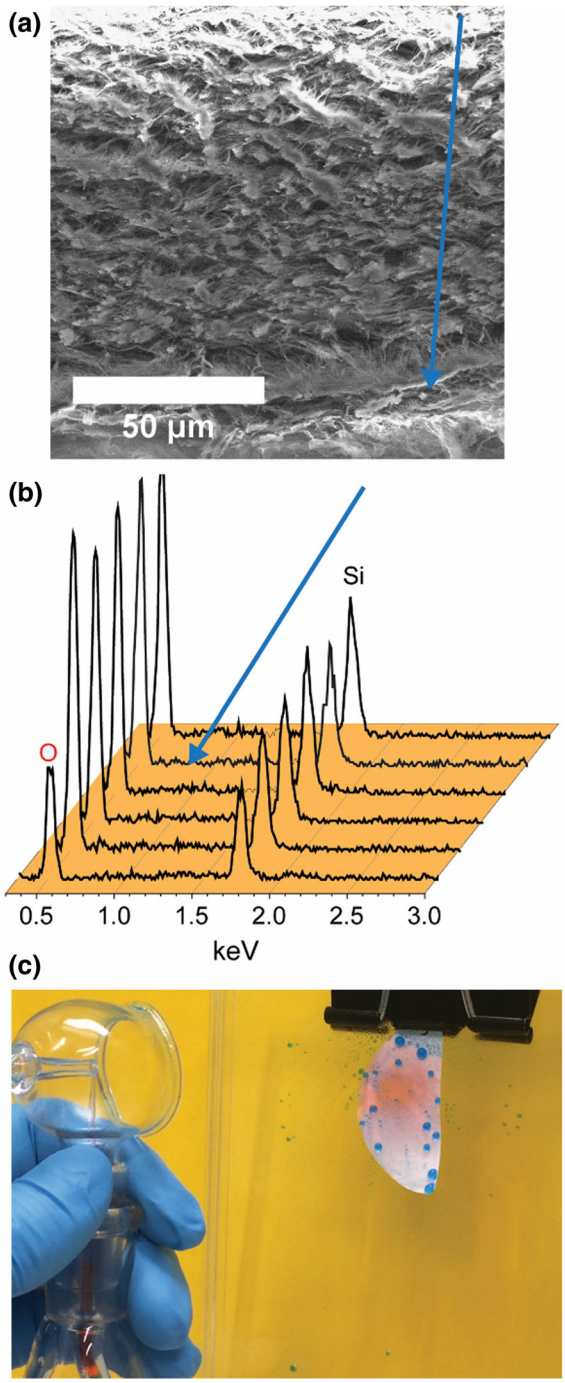

◀**Fig. 7** **a** SEM micrograph of a cross section of a porous film exposed to 0.4 M methyltrichlorosilane (the blue arrow indicates the position of an EDX line scan, from the top to the bottom surface); **b** EDX line-scan spectra of 6 points perpendicular to the film surface showing oxygen peak at 0.5 keV and Si peak at 1.7 keV; **c** exposure of a porous film treated with 0.025 M methyltrichlorosilane to a nebulized mixture of dodecane (red) and deionized water (blue): dodecane is absorbed, whereas water is repelled and slides down the surface (see corresponding Video MOV1). (Color figure online)

lyophilisation process of ice crystals (Jin et al. 2004). Foams, previously conditioned at 43%RH, were treated with increasing methyltrichlorosilane concentration in a toluene bath and analyzed by EDX in mapping mode.

We evaluated the presence of silicon, revealed by a peak appearing in all samples at 1.7 keV. Figure 8a shows that the ratio between the silicon and the oxygen peak intensity was about an order of magnitude higher at the surface than in the center of the cross section, independent on the methyltrichlorosilane concentration (viz. 0.025, 0.4 and 2.7 M). When considering the silicon mapping, one could visualize a heterogeneous distribution of Si at the cellulose foam surface (see Fig. 8b), while in the foam core the distribution was homogeneous (see Fig. 8c).

Scanning electron microscopy (SEM)

SEM images of foam surfaces treated with methyltrichlorosilane at different concentrations between 0.025 and 2.7 M (Fig. 9) reveal optimum conditions for formation of polysiloxane nanofilaments at intermediate methyltrichlorosilane concentrations (e.g. 0.4 M of MTCS concentration, Fig. $9b_{1-2}$). At these concentrations, polysiloxane nanofilaments were homogeneously distributed within the macropores of the NFC foams. Indeed, in the case of low methyltrichlorosilane concentrations (0.025 M, Fig. $9a_{1-2}$), polysiloxane nanofilaments were formed only on few regions of the foams, and at very high concentration (2.7 M, Fig. $9c_{1-2}$) a continuous layer of polysiloxane covered the foams. This continuous layer partially occluded the cellulose foam pores, thus causing an undesirable porosity reduction of the sample. When considering the structure of the foam (i.e. in the case of a MTCS concentration of 0.4 M) and comparing the top surface (Fig. 9d) with the core (Fig. 9e), polysiloxane filaments are observed at the surface but cannot be visualized in the center.

As the chemical reaction is performed in static conditions (no mixing) and diffusion governs enrichment of methyltrichlorosilane at the inner surfaces of

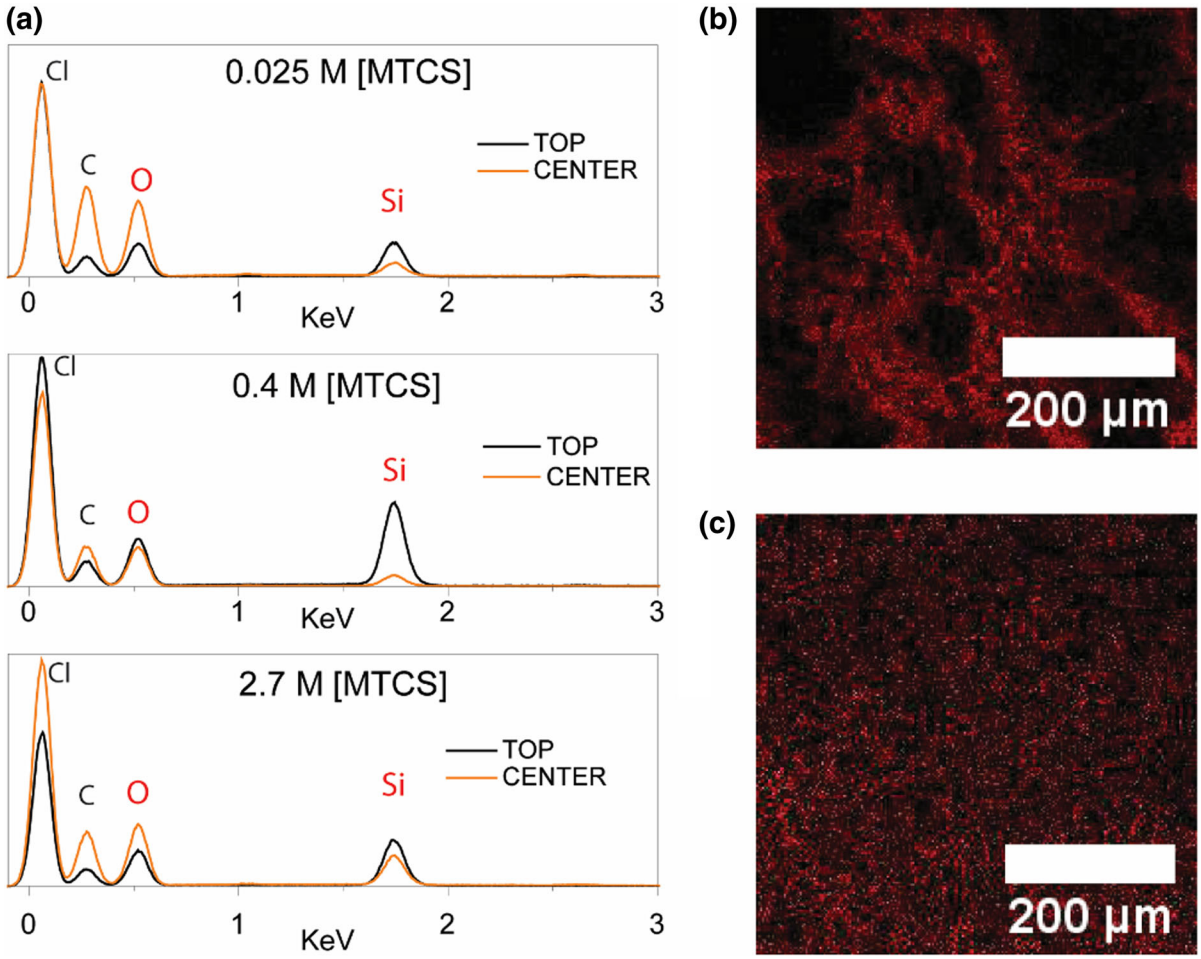

Fig. 8 EDX analysis of NFC foams exposed to various methyltrichlorosilane concentrations: **a** silicon (Si) and oxygen (O) contents of foams at the surface (TOP) and center (0.025, 0.4 and 2.7 M, top to bottom); **b** silicon mapping for a concentration of 0.4 M at the surface and **c** in the core

the foams, local methyltrichlorosilane gradients in the foam are expected. Thus, one could speculate that unreacted methyltrichlorosilane molecules were more prone to react with hydrolysis products of previously deposited methyltrichlorosilane at the surface region, rather than with hydroxyl groups in the unreacted cellulose core. This could be a consequence of the foams' high specific surface area and the relatively high thickness of the samples (about 1 cm), compared to the polysiloxane layer thickness. In the inner areas, where conditions of limited concentration for the formation of filaments occurred, the formation of very thin polysiloxane layers was probably favored. Figure 9d, e reveals similar silane features that could be recalled to the silicon mapping features obtained in Fig. 8b, c, respectively, confirming our explanation.

Dodecane absorption tests

To test the efficiency of the polysiloxane-modified foams in absorbing and retaining apolar compounds (SI, Figure S3), even in a polar environment (i.e. in water), dodecane absorption tests were performed. First, unmodified and modified foams were exposed to a dodecane bath and the absorbing capacity of dodecane was measured (Fig. 10a).

Foams demonstrated remarkable capabilities to absorb dodecane, with values of $\sim$ 60 $g_{dodecane}/g_{foam}$ (unmodified foam), and $\sim$ 50 $g_{dodecane}/g_{foam}$ for

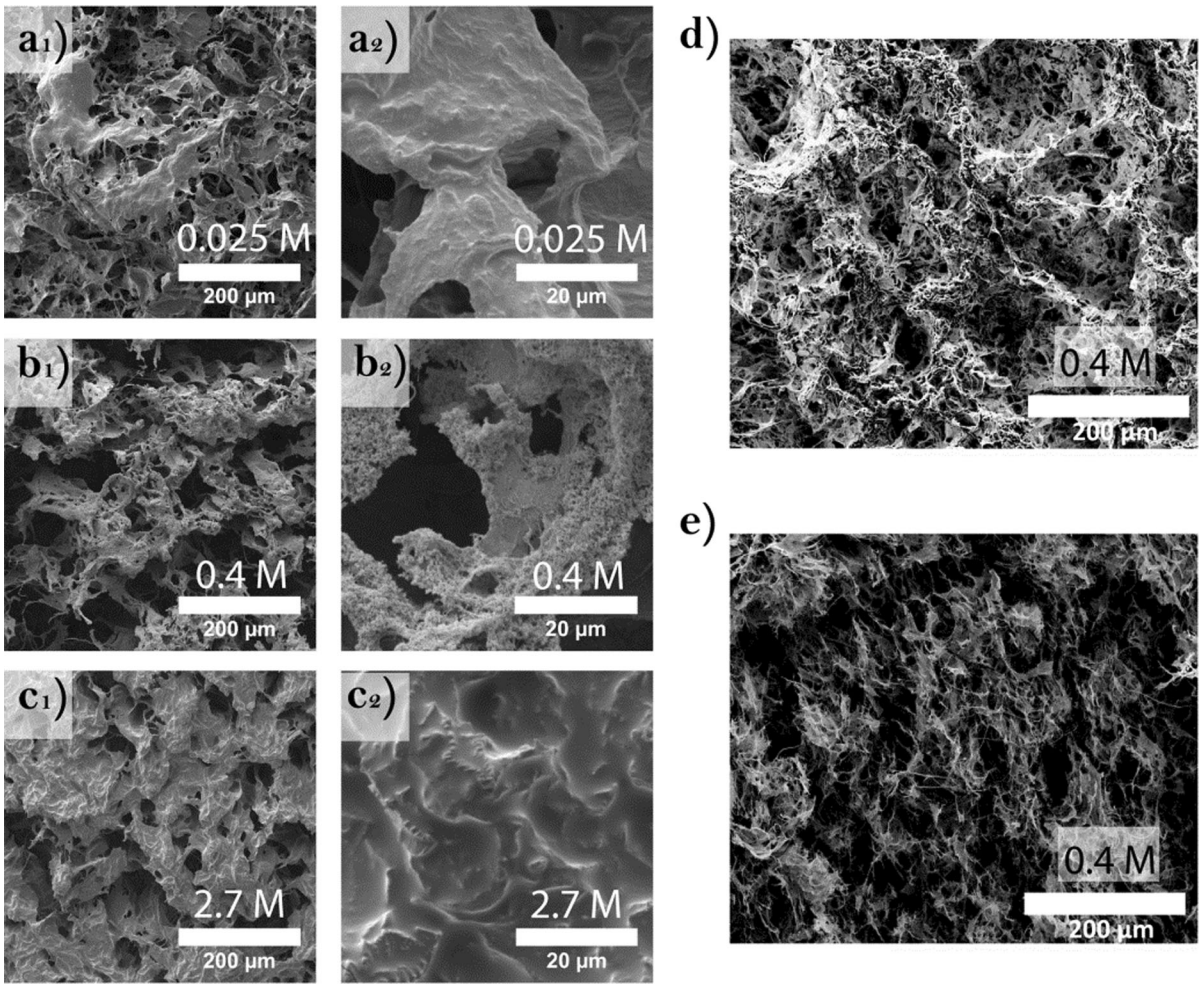

Fig. 9 Foam characterization: SEM images at two different magnifications showing the surface features after treatment with methyltrichlorosilane with a MTCS concentration of **a** 0.015 M, **b** 0.4 M and **c** 2.7 M; **d** SEM images top view and **e** cross section of foam modified with 0.4 M MTCS

foams functionalized at 0.025 and 0.1 M methyltrichlorosilane concentration. At higher silane concentrations, the dodecane absorbing capacity decreased strikingly, possibly because of the above mentioned pore occlusion. These results are coherent with absorption values of hydrocarbons and oil found for MTCS-modified chitin sponges (Duan et al. 2014) via a chemical vapor deposition approach, but in the present case a much simpler wet-chemistry approach has been used. After the absorption test, foams were immersed in water (Fig. 10b and SI, movie MOV2). Unmodified foams, despite possessing the highest absorption capacity, quickly released dodecane due to their higher affinity for water and broke down. At low methyltrichlorosilane concentrations (viz. 0.025 M), dodecane remained rather well absorbed, but the foam experienced breaking apart in water, possibly due to incomplete modification of some foam regions. In contrast, all other modified foams functionalized at methyltrichlorosilane concentrations of 0.1 M or higher did not release any noticeable trace of dodecane, the water remained clear (blue color), the dodecane remained fully absorbed in the NFC foam, and the foam did not break. As such, we can conclude that foams exposed to $\sim$ 0.1 M methyltrichlorosilane correspond to an optimal system for recovery of apolar compounds (including oils) for NFC, providing the best compromise between hydrocarbon absorption

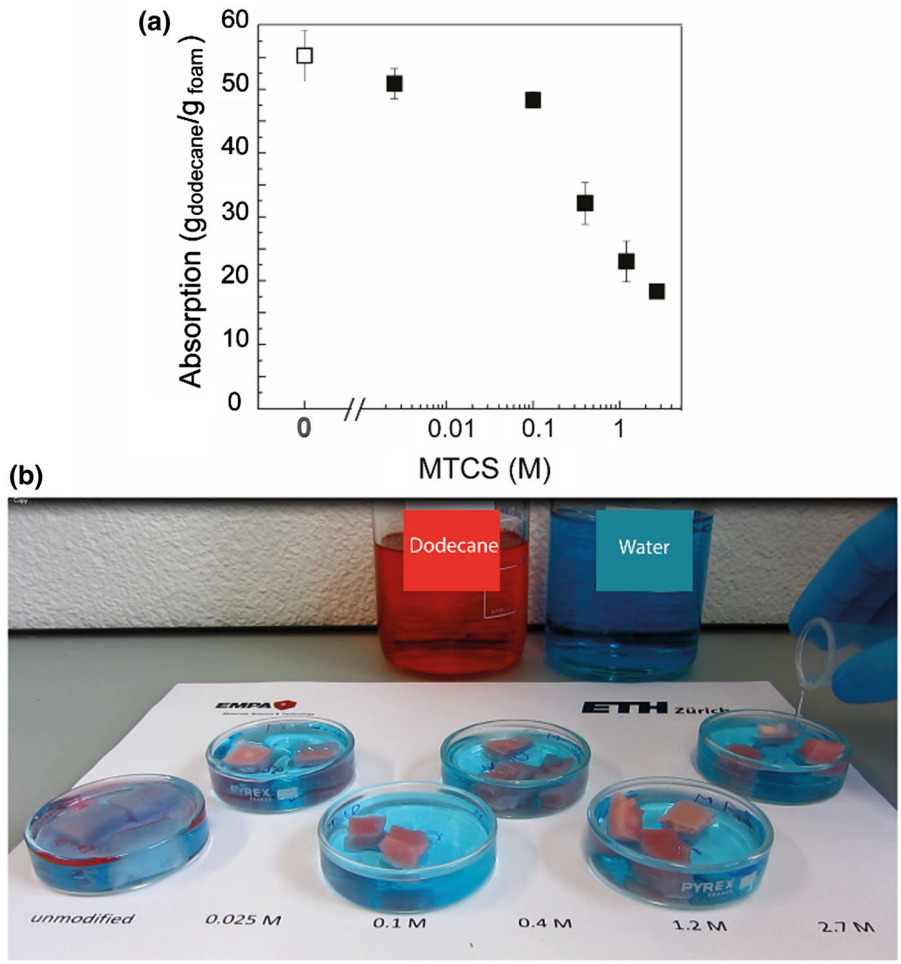

Fig. 10 **a** Dodecane absorption capacity expressed as $g_{dodecane}/g_{foam}$, for neat foam (open square) and foams exposed to different methyltrichlorosilane concentrations: 0.025, 0.1, 0.4, 1.2 and 2.7 M (closed squares); **b** pictures of foams exposed to various methyltrichlorosilane concentrations after uptake of dodecane containing a red dye floating on water containing a blue dye (see Supplemental Video, MOV2). (Color figure online)

capacity and integrity in water, as guaranteed by excellent superhydrophobicity. The retention ability of absorbed dodecane increased with increasing silane concentration. As shown in the movie MOV2 of the supplementary materials, for methyltrichlorosilane concentration of 0.1 M and above the foams are not only retaining the dodecane, but are also mechanically stable, i.e. they do not break apart. Foams modified with 0.1 and 0.4 M methyltrichlorosilane concentration were subjected to recyclability experiments of the dodecane absorption capacity upon six cycles. The absorption capacity was kept almost constant; specifically, for 0.1 M the values remained in the range of $\sim$ 50 $g_{dodecane}/g_{foam}$ and between 30 and 40 $g_{dodecane}/g_{foam}$ in the case of 0.4 M concentration (Supplementary Information, Figure S5).

Powders

Scanning electron microscopy (SEM)

Dispersed NFC fibers were also directly chemically modified in suspension by exposure to methyltrichlorosilane (see SEM images in Figure S6). Various concentrations were employed (viz. 0.006, 0.025 and 1 M methyltrichlorosilane), and no significant change was observed in the structure of the NFC modified powder (SI, Figure S4). Since higher concentration of silane did not bring additional structural benefit (viz. features) to the modification of the powder, the lowest concentration of 0.006 M can be considered the optimal one among these three. The formation of a polysiloxane coating on NFC and additional silicone nanofilaments propagating from

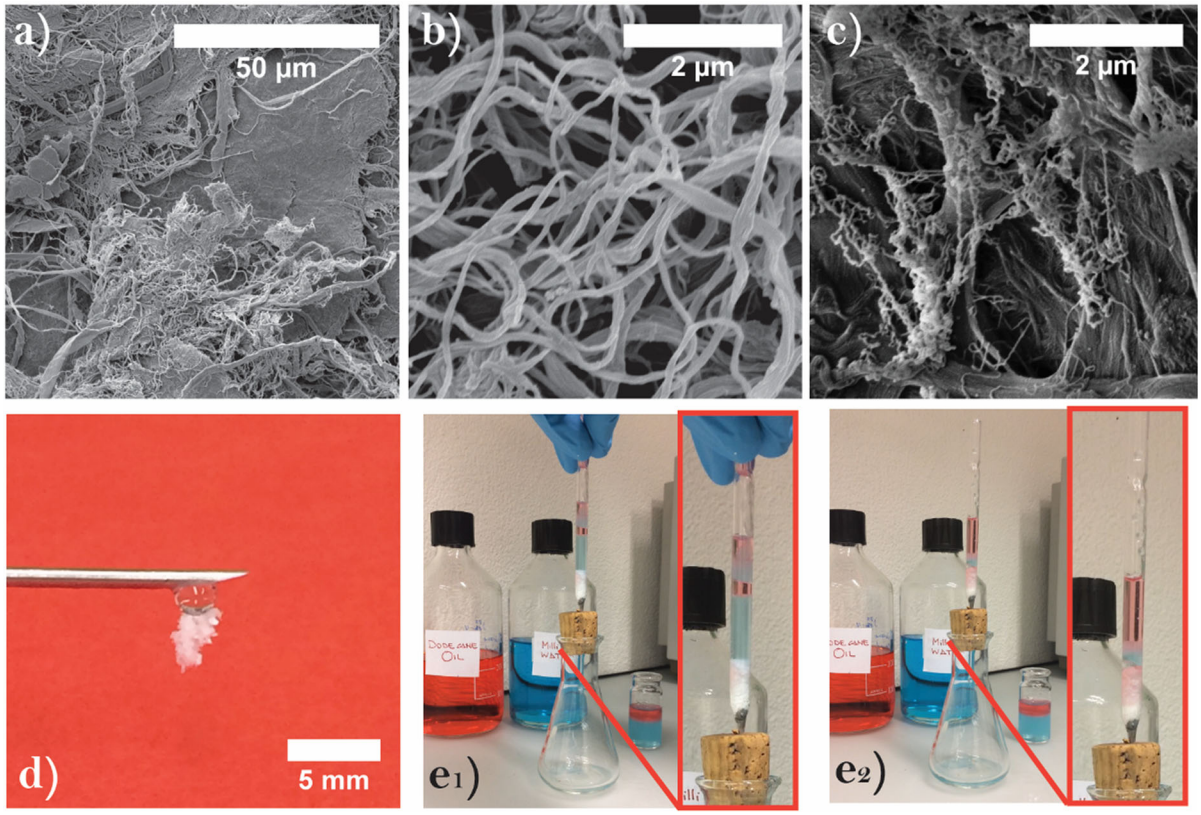

Fig. 11 NFC chemically modified by treatment with 0.006 M methyltrichlorosilane: **a** SEM micrograph providing an overview on the surface of the modified product, **b** details of the modified NFC fibers and **c** aggregates covered with polysiloxane nanofilaments; **d** photograph of modified nanofibers repelling a water drop at a needle tip; $\mathbf{e_1}$ photographs of a glass pipette filled with modified NFC and put in contact with a mixture of dodecane (red-stained) and water (blue-stained) taken before the fluid penetration in the modified nanofibers and $\mathbf{e_2}$ after the passage of water, collected in the flask, and the retention of dodecane in the modified NFC bed. (Color figure online)

the nanocellulose surface influenced the drying behavior of such nanomaterials: while unmodified NFC would undergo hornification (Eyholzer et al. 2010) and collapsing of the fibers into a compact layer, the methyltrichlorosilane-modified NFC resulted into a heterogeneous loose white powder, upon drying from ethanol. After modification the lack of available OH groups onto NFC, normally establishing hydrogen bonding and allowing the formation of continuous materials, resulted in a discrete powder and no further elaboration of films of foams was possible. Indeed, SEM images showed the formation of flocks of modified NFC aggregates (Fig. 11a) presenting both a coated filamentous material (Fig. 11b) and more compact regions decorated with free polysiloxane nanofilaments (Fig. 11c). We can speculate that residual water molecules, essential for the success of the chemical reaction, were evenly distributed on the unmodified fibers prior the reaction, resulting either in compacted flocks or in free filaments.

The powder showed water repellency, when put in contact with a water drop (Fig. 11d). To assess the repellency of modified NFC towards organic liquid, the material was loaded into a glass pipette to form a fiber bed and put in contact with a biphasic mixture of dodecane (red-stained) and water (blue-stained), as visualized in Fig. 11e_1. After a few seconds, the water penetrated through the modified NFC bed, while dodecane was retained on the modified NFC fibers, as shown by the powder color change, from white to red (Fig. 11e_2). A movie of the filtration experiments is available as supplementary material (SI, MOV3).

Solid-state NMR spectroscopy

The ^{1}H-^{13}C CP spectra of hydrophobized fibers (Fig. 12a, Figure S7a) display a band related to polysiloxane methyl groups (near 0 ppm), in addition to C1–C6 cellulose bands (60–105 ppm). The C4 and C6 bands display an additional peak or shoulder related to amorphous or surface cellulose (Larsson et al. 1997), as expected for NFC, but no systematic differences in the cellulose signals were observed as a function of silane loading (Figure S7a). The ^{1}H-^{29}Si CP spectra (Fig. 12b, Figure S7b) provide information on the T^n speciation, where T^n is a Si atom connected to one methyl group, *n* bridging oxygen atoms connected to *n* Si next-nearest neighbors, and 3-*n* non-bridging oxygen atoms. The NMR data do not resolve non-bridging oxygen atoms in the form of a ≡Si–OH group and ≡Si–O–C≡ bonds that link silane groups to cellulose. All investigated fibers contain between 55 and 70% of T^3 and between 45 and 30% of T^2 without systematic dependencies of silane content or speciation on the methyltrichlorosilane concentration in the hydrophobization solution (Figure S7, Table S1). About two thirds of the silane is fully polymerized and the remaining third also has two Si next-nearest neighbors. The ^{1}H-^{29}Si NMR data thus confirm that Si is present as large molecular polysiloxane entities or nanoscale structures, rather than as individual silane groups grafted onto the cellulose surfaces. It is not possible to accurately quantify the degree of substitution, i.e. the degree to which cellulose ≡C–OH has been replaced by ≡C–O–Si≡ during hydrophobization, but the NMR data do provide an estimate for the upper boundary: depending on the synthesis conditions, at most 1–6% of the total cellulose hydroxyl groups, corresponding to 21–97% of surface hydroxyl groups, have been substituted (Table S1). This upper boundary corresponds to a scenario where all T^2 groups are bonded to cellulose, and will thus significantly overestimate the true degree of substitution. The efficient hydrophobization of the cellulose fibers, and presumably also the membranes and foams, is thus not the result of a particularly high degree of substitution of surface hydroxyl groups but due to the formation of polysiloxane coatings and structures. These large polysiloxane clusters and structures, derived from trifunctional silanes, are grafted onto the cellulose surface through multiple ≡C–O–Si≡ bonds, and thus less likely to be removed than mono-functional silanes that can be removed through the hydrolysis of a single bond, e.g. ≡C–O–Si(CH_3) (Takeshita et al. 2017).

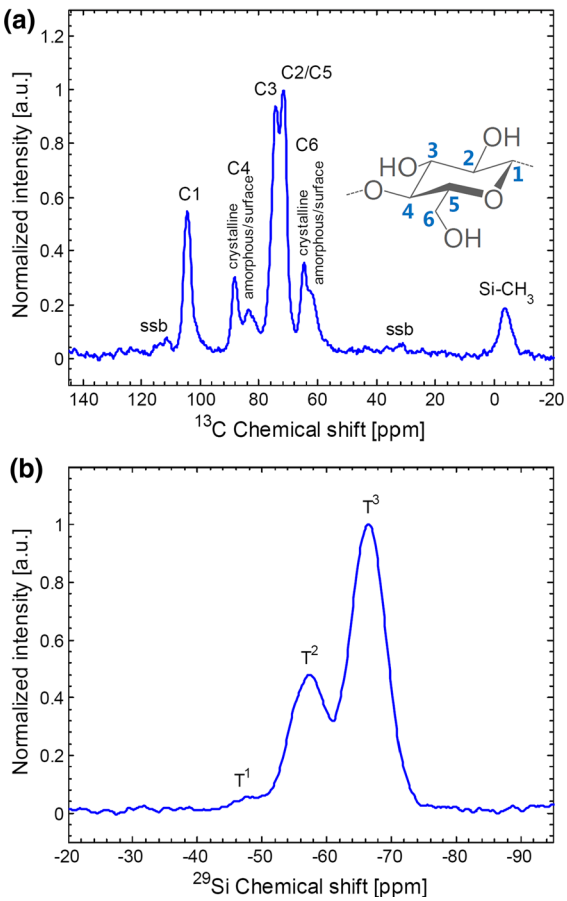

Fig. 12 Solid-state NMR spectra of NFC fibers hydrophobized with a 0.025 M MTCS solution (sample R3). **a** ^{1}H-^{13}C cross polarization (CP) spectrum. **b** ^{1}H-^{29}Si CP spectrum

Overall substrate comparison

We have shown that different cellulose-based substrates, including NFC dense films, porous films, foams and nanofibers were exposed to methyltrichlorosilane using the same chemical protocol. Each system showed superhydrophobic properties, which were reached at an optimal concentration of methyltrichlorosilane, depending on the substrate type. In all cases, contact angle values of about 160° were obtained after ultrasonication of samples, independently from the specific surface texture; other "bulk" properties, such as total pore volume in the

foams, only play a role in the maximum uptake ability of hydrocarbons as potential space to allocate higher amounts of liquids but did not affect the wetting properties. Moreover, foams retained their properties upon several absorbing/recycling cycles in toluene, indirectly demonstrating the stability of the modification.

Thermogravimetric analysis (TGA)

To evaluate the silicon content, TGA measurements were performed under both nitrogen and air atmosphere (Fig. 13). While for modified NFC foams there was a sensible increase in the residual mass with increasing methyltrichlorosilane concentration (Fig. 13a), no differences were observed for porous films, with a constant residue of ca. 20% (Fig. 13b), and for powders, with residue of ∼ 10 to 15% (Fig. 13c). This trend is in agreement with the aforementioned considerations. The formation of a bulk methyltrichlorosilane layer on foams was observed at high MTCS content, showing a substantial silane uptake covering and occluding the foam porosity (Fig. 13c); this was also confirmed by the reduced dodecane uptake for higher MTCS concentration (Fig. 13): indeed, for methyltrichlorosilane concentration of 1.2 and 2.7 M, high residues of 40 and 60% were determined. In the case of porous films, no significant differences were found for the wetting behavior (viz. contact angle, Fig. 13) and the silicon

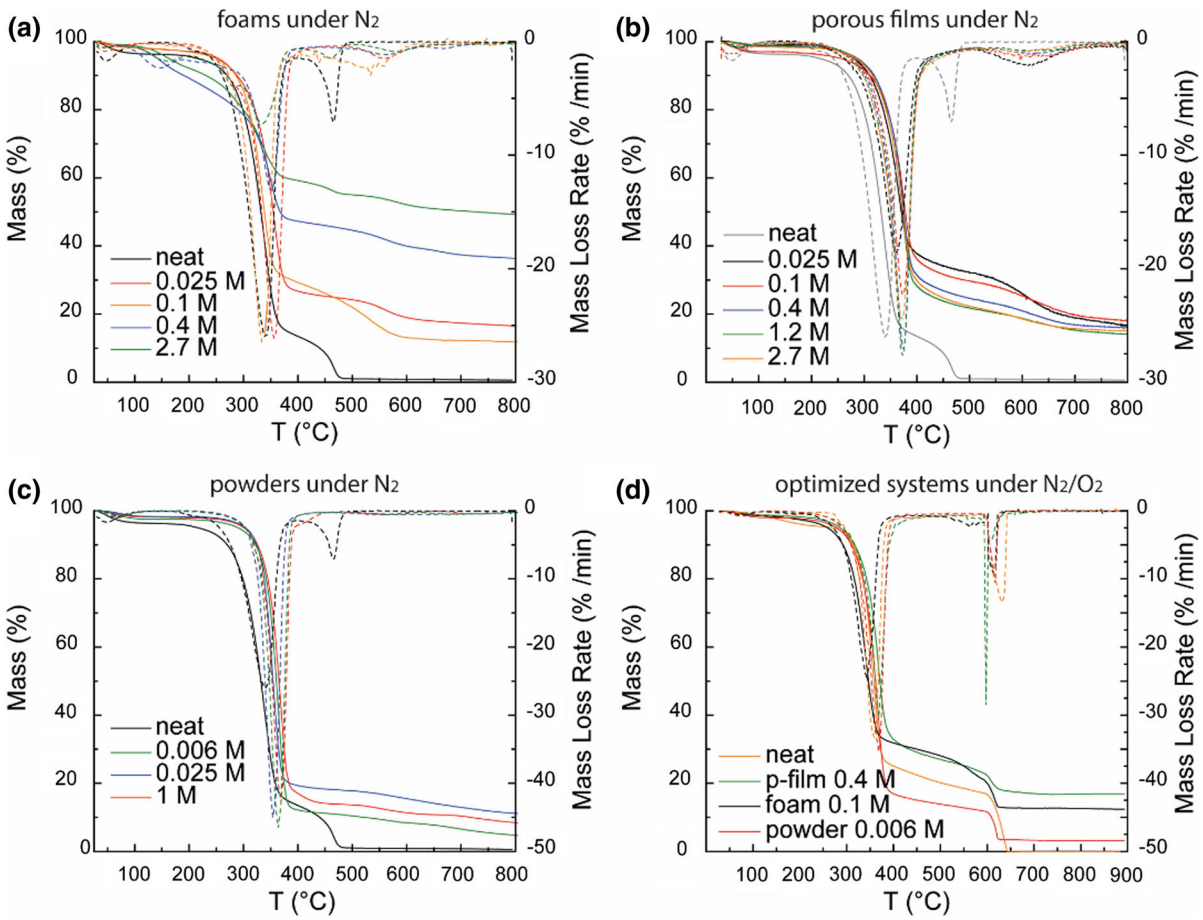

Fig. 13 Mass loss (continuous lines) and mass loss derivative (dashed lines) derived from thermogravimetric analysis executed on the MTCS-modified substrates: **a** thermograms for foams under N_2; **b** thermograms for porous films under N_2; **c** thermograms for powders of modified NFC under N_2; **d** thermograms obtained under N_2 up to 600 °C and switching to O_2 up 900 °C for optimized systems (viz. porous films at 0.4 M MTCS, foams at 0.1 M MTCS and powders at 0.006 M MTCS)

distribution (viz. Figure S2) in the materials, suggesting that for increasing methyltrichlorosilane concentration, no increase in deposited polysiloxane occurred and no additional benefit in wetting performance could be observed.

SEM images (Figure S4) did not show substantial differences for NFC powders treated with increasing methyltrichlorosilane concentrations. From our investigation, we could define that each substrate had an optimum methyltrichlorosilane concentration as follows: for dense films 0.1–0.4 M, for porous films 0.4 M, for foams 0.1 M and for powders 0.006 M. The thermal stability of these materials was analyzed not only under nitrogen, but also under air atmosphere, to combust the cellulose fraction and to determine the final silicon content (Fig. 13d): we found respectively residual silicon for values amounting to 16% for porous films, to 12% for foams and to 3% for powders, consistent with the estimates from the solid-state NMR data (Table S1). As expected, the reference unmodified (viz. neat) NFC sample had no residue after combustion.

Conclusions

In this work, we demonstrated the effective functionalization of NFC-based materials to promote superhydrophobicity on an intrinsically hydrophilic natural polymer, i.e. cellulose, extending the approach initially proposed of Gao and McCarthy (2006) for inorganic glass substrates. By using the same ingredients, largely available materials, such as NFC and methyltrichlorosilane, and developing similar processes (solution based chemical modification in toluene), different functional and high-performance superhydrophobic materials were developed, targeting environmental remediation operations.

These materials distinguish de facto in the distribution of the polysiloxane on the NFC porous and dense films. As such, NFC dense films obtained by vacuum filtration, porous films by supercritical drying, foams by freeze-drying and centrifuged powders were functionalized revealing superhydrophobicity after modification by methyltrichlorosilane, as a result of hydrophobic nanofilament formation, due to MTCS polymerization.

The novelty of the work is multifaceted and is related to various aspects: (1) the enhancement of the wetting properties, from hydrophilic to superhydrophobic; (2) the combination of two materials with nanoscale features (nanocellulose and nanofilaments), providing multi-tier topography and unprecedented wetting characteristics; (3) the independence of the treatment from substrate nature (dense or porous films, foams, filaments); (4) the evaluation of the optimal conditions for polysiloxane nanofilaments growth, with identification of various regimes of coating versus nanofilaments growth, and finally (5) the demonstration of multiple applications for superhydrophobic nanocellulose materials, which include liquid-infused surfaces, selective absorption foams, and filters for dodecane/water separation. As such, we demonstrated the high potential of methyltrichlorosilane functionalization for tailoring wetting properties of NFC-based materials, providing a wide spectrum of different applications, where preferential liquid wetting capabilities can be used to control liquid mixture (e.g. water/hydrocarbon) behavior at interfaces.

Acknowledgments Dr. P. Tingaut and Dr. T. Geiger are kindly acknowledged for fruitful scientific discussions. We kindly acknowledge Empa colleagues B. Fischer for TGA measurements, E. Strub for SEM imaging, A. Huch for SEM/EDX imaging, and M. Koebel for providing access to the Karl-Fischer titration device and other laboratory facilities.

Author's contribution The manuscript was written through contributions of all authors. PO and CA designed and carried out the experimental work related to dense films, porous films and foams. PO and AS performed nanofiber chemical modification and characterization. CA performed contact angle measurements. WJM performed the solid-state NMR analysis and interpretation. WRC and TZ supervised the scientific activities throughout the entire work. All authors have given approval to the final version of the manuscript.

Funding EMPA is kindly acknowledged for internal funding.

References

Anand S, Paxson AT, Dhiman R et al (2012) Enhanced condensation on lubricant-impregnated nanotextured surfaces. ACS Nano 6:10122–10129. https://doi.org/10.1021/nn303867y

Antonini C, Villa F, Bernagozzi I et al (2013) Drop rebound after impact: the role of the receding contact angle. Langmuir. https://doi.org/10.1021/la4012372

Artus GRJ, Seeger S (2014) One-dimensional silicone nanofilaments. Adv Colloid Interface Sci 209:144–162

Artus GRJ, Jung S, Zimmermann J et al (2006) Silicone nanofilaments and their application as superhydrophobic coatings. Adv Mater 18:2758–2762

Bormashenko EY (2013) Wetting of real surfaces. Walter de Gruyter, Berlin/Boston

Cervin NT, Aulin C, Larsson PT, Wågberg L (2012) Ultra porous nanocellulose aerogels as separation medium for mixtures of oil/water liquids. Cellulose 19:401–410. https://doi.org/10.1007/s10570-011-9629-5

Cunha AG, Freire C, Silvestre A et al (2010) Preparation of highly hydrophobic and lipophobic cellulose fibers by a straightforward gas-solid reaction. J Colloid Interface Sci 344:588–595. https://doi.org/10.1016/j.jcis.2009.12.057

Duan B, Gao H, He M, Zhang L (2014) Hydrophobic modification on surface of chitin sponges for highly effective separation of oil. ACS Appl Mater Interfaces 6:19933–19942. https://doi.org/10.1021/am505414y

Eyholzer C, Bordeanu N, Lopez-Suevos F et al (2010) Preparation and characterization of water-redispersible nanofibrillated cellulose in powder form. Cellulose 17:19–30. https://doi.org/10.1007/s10570-009-9372-3

Flemming M, Coriand L, Duparré A (2009) Ultra-hydrophobicity through stochastic surface roughness. J Adhes Sci Technol 23:381–400. https://doi.org/10.1163/156856108X370082

Gao L, McCarthy TJ (2006) A perfectly hydrophobic surface (θA/θR = 180°/180°). J Am Chem Soc 128:9052–9053. https://doi.org/10.1021/ja062943n

Guo J, Fang W, Welle A et al (2016) Superhydrophobic and slippery lubricant-infused flexible transparent nanocellulose films by photoinduced thiol-ene functionalization. ACS Appl Mater Interfaces 8:34115–34122. https://doi.org/10.1021/acsami.6b11741

Jiao Y, Wan C, Qiang T, Li J (2016) Synthesis of superhydrophobic ultralight aerogels from nanofibrillated cellulose isolated from natural reed for high-performance adsorbents. Appl Phys A 122:1–10. https://doi.org/10.1007/s00339-016-0194-5

Jin H, Nishiyama Y, Wada M, Kuga S (2004) Nanofibrillar cellulose aerogels. Colloids Surf A 240:63–67. https://doi.org/10.1016/j.colsurfa.2004.03.007

Jin H, Kettunen M, Laiho A et al (2011a) Superhydrophobic and superoleophobic nanocellulose aerogel membranes as bioinspired cargo carriers on water and oil. Langmuir 27:1930–1934. https://doi.org/10.1021/la103877r

Jin M, Wang J, Hao Y et al (2011b) Tunable geometry and wettability of organosilane nanostructured surfaces by water content. Polym Chem 2:1658. https://doi.org/10.1039/c1py00246e

Khoo HS, Tseng F-G (2008) Engineering the 3D architecture and hydrophobicity of methyltrichlorosilane nanostructures. Nanotechnology 19:345603. https://doi.org/10.1088/0957-4484/19/34/345603

Kim SH (2008) Fabrication of superhydrophobic surfaces. J Adhes Sci Technol 22:235–250. https://doi.org/10.1163/156856108X305156

Korhonen JT, Kettunen M, Ras RH, Ikkala O (2011) Hydrophobic nanocellulose aerogels as floating, sustainable, reusable, and recyclable oil absorbents. ACS Appl Mater Interfaces 3:1813–1816. https://doi.org/10.1021/am200475b

Lafuma A, Quere D (2003) Superhydrophobic states. Nat Mater 2:457–460

Larsson PT, Wickholm K, Iversen T (1997) A CP/MAS 13C NMR investigation of molecular ordering in celluloses. Carbohydr Res 302:19–25. https://doi.org/10.1016/S0008-6215(97)00130-4

Lavoine N, Desloges I, Dufresne A, Bras J (2012) Microfibrillated cellulose—its barrier properties and applications in cellulosic materials: a review. Carbohydr Polym 90:735–764. https://doi.org/10.1016/j.carbpol.2012.05.026

Li W, Amirfazli A (2005) A thermodynamic approach for determining the contact angle hysteresis for superhydrophobic surfaces. J Colloid Interface Sci 292:195–201. https://doi.org/10.1016/j.jcis.2005.05.062

Maitra T, Antonini C, Auf der Mauer M et al (2014) Hierarchically nanotextured surfaces maintaining superhydrophobicity under severely adverse conditions. Nanoscale 6:8710–8719. https://doi.org/10.1039/c4nr01368a

Malfait WJ, Zhao S, Verel R et al (2015) Surface chemistry of hydrophobic silica aerogels. Chem Mater 27:6737–6745. https://doi.org/10.1021/acs.chemmater.5b02801

Nishino T, Meguro M, Nakamae K et al (1999) The lowest surface free energy based on –CF 3 alignment. Langmuir 15:4321–4323

Oh SY, Il Yoo D, Shin Y et al (2005) Crystalline structure analysis of cellulose treated with sodium hydroxide and carbon dioxide by means of X-ray diffraction and FTIR spectroscopy. Carbohydr Res 340:2376–2391

Orsolini P, Michen B, Huch A et al (2015) Characterization of pores in dense nanopapers and nanofibrillated cellulose membranes: a critical assessment of established methods. ACS Appl Mater Interfaces 7:25884–25897. https://doi.org/10.1021/acsami.5b08308

Patankar N (2009) Hydrophobicity of surfaces with cavities. In: Taylor and Francis Group (ed) Superhydrophobic surfaces. CRC Press, London, pp 51–71

Payne KC, Jackson CD, Aizpurua CE et al (2012) Oil spills abatement: factors affecting oil uptake by cellulosic fibers. Environ Sci Technol 46:7725–7730. https://doi.org/10.1021/es3015524

Rioboo R, Marengo M, Tropea C (2002) Time evolution of liquid drop impact onto solid, dry surfaces. Exp Fluids 33:112–124. https://doi.org/10.1007/s00348-002-0431-x

Rioboo R, Delattre B, Duvivier D et al (2012) Superhydrophobicity and liquid repellency of solutions on polypropylene. Adv Colloid Interface Sci 175:1–10. https://doi.org/10.1016/j.cis.2012.03.003

Rockland LB (1960) Saturated salt solutions for static control of relative humidity between 5 and 40 C. Anal Chem 32:1375–1376. https://doi.org/10.1021/ac60166a055

Rykaczewski K, Anand S, Subramanyam SB, Varanasi KK (2013) Mechanism of frost formation on lubricant-impregnated surfaces. Langmuir 29:5230–5238. https://doi.org/10.1021/la400801s

Sai H, Fu R, Xing L et al (2015) Surface modification of bacterial cellulose aerogels' web-like skeleton for oil/water separation. ACS Appl Mater Interfaces 7:7373–7381. https://doi.org/10.1021/acsami.5b00846

Samyn P (2013) Wetting and hydrophobic modification of cellulose surfaces for paper applications. J Mater Sci

48:6455–6498. https://doi.org/10.1007/s10853-013-7519-y
Schellenberger F, Encinas N, Vollmer D, Butt HJ (2016) How water advances on superhydrophobic surfaces. Phys Rev Lett. https://doi.org/10.1103/PhysRevLett.116.096101
Smith JD, Dhiman R, Anand S et al (2013) Droplet mobility on lubricant-impregnated surfaces. Soft Matter 9:1772–1780
Spence KL, Venditti RA, Rojas OJ et al (2011) Water vapor barrier properties of coated and filled microfibrillated cellulose composite films. BioResources 6:4370–4388
Stojanovic A (2014) Polysiloxane nanostructures and their applications. University of Zurich, Zurich
Stojanovic A, Olveira S, Fischer M, Seeger S (2013) Polysiloxane nanotubes. Chem Mater 25:2787–2792. https://doi.org/10.1021/cm400851k
Syverud K, Stenius P (2009) Strength and barrier properties of MFC films. Cellulose 16:75–85. https://doi.org/10.1007/s10570-008-9244-2
Takeshita S, Yoda S, Dunlop N et al (2017) Translucent, hydrophobic, and mechanically tough aerogels constructed from trimethylsilylated chitosan nanofibers. Nanoscale 9:12311–12315. https://doi.org/10.1039/C7NR04051B
Tejado A, Chen WC, Alam MN, van de Ven TGM (2014) Superhydrophobic foam-like cellulose made of hydrophobized cellulose fibres. Cellulose 21:1735–1743. https://doi.org/10.1007/s10570-014-0247-x
van Beek JD (2007) matNMR: a flexible toolbox for processing, analyzing and visualizing magnetic resonance data in Matlab. J Magn Reson 187:19–26. https://doi.org/10.1016/j.jmr.2007.03.017
Wong T-S, Kang SH, Tang SKY et al (2011) Bioinspired self-repairing slippery surfaces with pressure-stable omniphobicity. Nature 477:443–447
Zhang J, Seeger S (2011) Polyester materials with superwetting silicone nanofilaments for oil/water separation and selective oil absorption. Adv Funct Mater 21:4699–4704. https://doi.org/10.1002/adfm.201101090
Zhang X, Shi F, Niu J et al (2008) Superhydrophobic surfaces: from structural control to functional application. J Mater Chem 18:621–633. https://doi.org/10.1039/B711226B
Zhang Z, Sèbe G, Rentsch D et al (2014) Ultralightweight and flexible silylated nanocellulose sponges for the selective removal of oil from water. Chem Mater 26:2659–2668. https://doi.org/10.1021/cm5004164
Zhao S, Zhang Z, Sèbe G et al (2015) Multiscale assembly of superinsulating silica aerogels within silylated nanocellulosic scaffolds: improved mechanical properties promoted by nanoscale chemical compatibilization. Adv Funct Mater 25:2326–2334
Zheng Q, Cai Z, Gong S (2014) Green synthesis of polyvinyl alcohol (PVA)-cellulose nanofibril (CNF) hybrid aerogels and their use as superabsorbents. J Mater Chem A 2:3110–3118. https://doi.org/10.1039/C3TA14642A
Zhou X, Zhang Z, Xu X et al (2013) Robust and durable superhydrophobic cotton fabrics for oil/water separation. ACS Appl Mater Interfaces 5:7208–7214. https://doi.org/10.1021/am4015346
Zimmermann J, Reifler FA, Fortunato G et al (2008) A simple, one-step approach to durable and robust superhydrophobic textiles. Adv Funct Mater 18:3662–3669